First-principles calculation of ground and excited-state absorption spectra of ruby and alexandrite considering lattice relaxation

Shinta Watanabe, Tomomi Sasaki, Rie Taniguchi, Takugo Ishii, and Kazuyoshi Ogasawara
Department of Chemistry, School of Science and Technology, Kwansei Gakuin University, 2-1 Gakuen, Sanda, Hyogo 669-1337, Japan
(Received 28 August 2008; published 11 February 2009)

We performed first-principles calculations of multiplet structures and the corresponding ground-state absorption and excited-state absorption spectra for ruby ($Cr^{3+}:\alpha$-Al_2O_3) and alexandrite ($Cr^{3+}:BeAl_2O_4$) which included lattice relaxation. The lattice relaxation was estimated using the first-principles total energy and molecular-dynamics method of the CASTEP code. The multiplet structure and absorption spectra were calculated using the configuration-interaction method based on density-functional calculations. For both ruby and alexandrite, the theoretical absorption spectra, which were already in reasonable agreement with experimental spectra, were further improved by consideration of lattice relaxation. In the case of ruby, the peak positions and peak intensities were improved through the use of models with relaxations of 11 or more atoms. For alexandrite, the polarization dependence of the U band was significantly improved, even by a model with a relaxation of only seven atoms.

DOI: 10.1103/PhysRevB.79.075109 PACS number(s): 78.20.−e, 71.15.Mb, 71.55.−i, 61.72.−y

I. INTRODUCTION

Crystals doped with trivalent chromium ions (Cr^{3+}) have been widely studied from both basic and applied perspectives. Among these materials, ruby ($Cr^{3+}:\alpha$-Al_2O_3), chromium-doped corundum, alexandrite ($Cr^{3+}:BeAl_2O_4$), and chromium-doped chrysoberyl are well known as gemstones and solid-state laser media. Ruby is especially well known since it was the medium used in the first solid-state laser ever developed[1] and it has been widely studied in the field of high-pressure science.[2–5] Alexandrite is known as a tunable solid-state laser. The laser action occurs not only on the R line but also on the vibronic sideband, and the lasing is broadly tunable.[6]

To date, ligand-field theory has been widely used and successfully employed in explaining the origins of optical spectra and multiplet energy levels of transition-metal (TM) ions in various crystals.[7] However, since ligand-field theory requires several empirical parameters, such as the Racah parameters or crystal-field parameters, it can be applied only to materials for which experimental optical data are available. In addition, the physical meanings of these empirical parameters are somewhat ambiguous because the effects of covalency and electron correlations are absorbed into them during the fitting process.

On the other hand, first-principles analysis of the electronic structure for TM impurities in crystals based on the density-functional theory (DFT) has recently been dramatically improved. These methods are quite useful for estimation of structural or optical properties on the basis of structural features.[8–15] However, since most of these analyses are based on the one-electron approximation, it is difficult to estimate the absolute multiplet energy and transition probability between multiplets. Therefore, first-principles calculation of the multiplet energy levels or transition probability between multiplets based on explicit many-electron wave functions, which is necessary to understand optical properties in detail, remains limited having only been performed by several groups.[16–21]

The Shannon's ionic radius of the trivalent aluminum ion (Al^{3+}) is about 115% larger than that of the trivalent chromium ion (Cr^{3+}).[22] The lattice relaxation caused by this substitution was reported based on experiments employing extended x-ray-absorption fine structure (EXAFS) analysis.[13,14,23] Since the covalency of the Al-O bond in α-Al_2O_3 cannot be neglected,[24] it is quite important to estimate the lattice relaxation caused by substitution of Al^{3+} by Cr^{3+} without any empirical parameters.

Previously, our group performed first-principles calculations of the multiplet energy levels and the corresponding ground-state absorption (GSA) spectra for Cr^{3+} and V^{3+} in α-Al_2O_3 which reasonably reproduced experimental observations, even though lattice relaxation was not considered.[19] In this paper, we performed more detailed investigations of both the GSA and excited-state-absorption (ESA) spectra as well as the absolute multiplet energy levels of ruby ($Cr^{3+}:\alpha$-Al_2O_3) and alexandrite ($Cr^{3+}:BeAl_2O_4$) by the first-principles method. In order to estimate the lattice relaxation caused by substitution of Al by Cr, we carried out first-principles calculations using the CASTEP code.[25,26] Using this method, we estimated the range of relaxation effects by substitution. In addition, we quantitatively investigated the polarization properties of both GSA and ESA spectra for ruby and alexandrite.

II. COMPUTATIONAL PROCEDURE

A. Estimation of lattice relaxation

The crystal structures of ruby and alexandrite are commonly known as corundum and chrysoberyl, respectively.[27,28] The crystal structures of each crystal are shown in Fig. 1 and the lattice parameters of each crystal are listed in Table I. Unfortunately, our cluster approach mentioned in Sec. II B cannot currently be applied to calculation of forces and stresses. In contrast, the band-structure approach, based on a pseudopotential plane-wave method, is very useful for calculation of forces and stresses. Accordingly, the structural

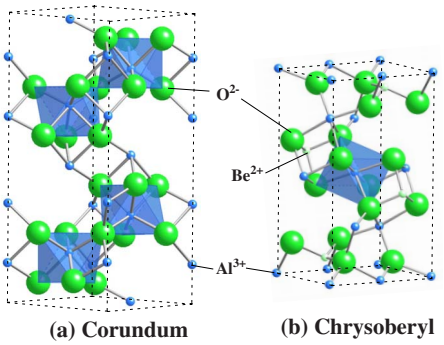

FIG. 1. (Color online) The crystal structures of corundum and alexandrite.

optimization calculations were performed using the band-structure approach instead of the cluster approach used in the calculation of multiplets and spectra. We performed a structural optimization around Cr^{3+} in α-Al_2O_3 and $BeAl_2O_4$ using a first-principles total-energy calculation with the CASTEP code,[25,26] which is based on the ultrasoft pseudopotential plane-wave (USPP) method. We adopted Vanderbilt[29] ultrasoft pseudopotentials throughout the present work. The orbitals explicitly treated as the valence state were $3s$, $3p$, calculated with the $3s^2 3p^1$ configuration and a core radius of 2.00 a.u. for Al; $2s$, calculated with the $2s^1$ configuration and a core radius of 2.00 a.u. for Be; $2s$, $2p$ calculated with the $2s^2 2p^4$ configuration and a core radius of 1.00 a.u. for O; and $3s$, $3p$, $3d$, $4s$ calculated with the $3s^2 3p^6 3d^{3.75} 4s^2$ configuration and a core radius of 1.80 a.u. for Cr. The exchange-correlation potential was considered within the generalized gradient approximation (GGA) proposed by Perdew, Burke, and Ernzerhof (PBE).[30] In order to evaluate the accuracy of the structural optimization, the lattice parameters and atomic positions in the unit cell of pure α-Al_2O_3 and $BeAl_2O_4$ crystals were optimized by this approach and compared to experimental values. In the case of α-Al_2O_3, we began the geometry optimization with 12 Al atoms at $(0,0,0;\frac{1}{3},\frac{2}{3},\frac{2}{3};\frac{2}{3},\frac{1}{3},\frac{1}{3})+(0,0,z;0,0,\bar{z};0,0\frac{1}{2}+z;0,0\frac{1}{2}-z)$, where $z=0.3522$, and 18 O atoms at $(0,0,0;\frac{1}{3},\frac{2}{3},\frac{2}{3};\frac{2}{3},\frac{1}{3},\frac{1}{3})+(x,0,\frac{1}{4};0,x,\frac{1}{4};\bar{x},\bar{x},\frac{1}{4};\bar{x},0,\frac{3}{4};0,\bar{x},\frac{3}{4};x,x,\frac{3}{4})$, where $x=0.3063$.[27] For $BeAl_2O_4$, we began the geometry optimization with four C_i site Al atoms at $(0,0,0;0,\frac{1}{2},0;\frac{1}{2},0,\frac{1}{2};\frac{1}{2},\frac{1}{2},\frac{1}{2})$ and with four C_s site Al atoms at $\pm(x,\frac{1}{4},z;\frac{1}{2}+x,\frac{1}{4},\frac{1}{2}-z)$, where $x=0.2732$, $z=0.9941$. Four Be atoms, four O1 atoms, and four O2 atoms were also located on mirror plane sites. The initial values of x and z parameters were $x=0.0929$ and $z=0.4335$ for Be, $x=0.0905$ and $z=0.7902$ for O1, and $x=0.4334$ and $z=0.2410$ for O2. In addition, eight O3 atoms were located in general positions at $\pm(x,y,z;\frac{1}{2}+x,\frac{1}{2}-y,\frac{1}{2}-z;x,\frac{1}{2}-y,z;\frac{1}{2}+x,y,\frac{1}{2}-z)$, where $x=0.1632$, $y=0.0172$, and $z=0.2585$.[28] Respective parameters are tabulated in Table II. In these host crystal calculations, the cutoff energy of the plane wave was 390 eV and the Brillouin zone was sampled on the $6\times6\times4$ and $4\times6\times6$ Monkhorst-Pack grids for ruby and alexandrite, respectively. We then constructed a $2\times2\times2$ rhombohedral supercell for ruby, which consisted of 80 atoms, and a $1\times2\times1$ supercell for alexandrite, which consisted of 56 atoms using the calculated structure and a Cr^{3+} ion doped to one Al^{3+} site in each supercell. In these supercell calculations, the cutoff energy of the plane wave was 390 eV and the Brillouin zone was sampled on the $3\times3\times3$ and $3\times2\times6$ Monkhorst-Pack grids for ruby and alexandrite, respectively. The numerical error was estimated to be less than 1 meV/atom by cutoff and k-point convergence tests. In alexandrite, there are two types of Al^{3+} sites: the inversion symmetry site (C_i site) and the reflection symmetry site (C_s site). Although the lattice relaxation was estimated for both symmetries, since the electric-dipole transition is forbidden at the C_i site, the theoretical spectra were calculated only for C_s. In these calculations, the atomic positions of a doped Cr atom and the surrounding O and Al atoms were relaxed in several patterns in order to estimate the range of the lattice relaxation effect. For ruby, we estimated the optimized structure in three patterns. We calculated the lattice relaxation of atomic positions for (1) a doped Cr atom and the nearest six O atoms, (2) a doped Cr atom and the nearest six O and four Al atoms, and (3) a doped Cr atom and the nearest six O and 13 Al atoms. For alexandrite, we estimated the optimized structure in two patterns: (1) a doped Cr atom and the nearest six O atoms and (2) a doped Cr atom and the nearest six O, ten Al, and four Be atoms. Geometry optimization was performed until the residual forces and stresses dropped below 0.01 eV/Å and 0.02 GPa, respectively.

TABLE I. Theoretical and experimental lattice parameters of α-Al_2O_3 and $BeAl_2O_4$.

	Calculation (Å)	Experiment (Å)[a]	Ratio (%)
α-Al_2O_3 a and b axes	4.7020	4.7571	98.8
α-Al_2O_3 c axis	12.9887	12.8683	99.1
$BeAl_2O_4$ a axis	9.402	9.404	100.0
$BeAl_2O_4$ b axis	5.457	5.476	100.3
$BeAl_2O_4$ c axis	4.426	4.427	100.0

[a]References 27 and 28.

TABLE II. Theoretical and experimental values of internal coordinates for α-Al_2O_3 and $BeAl_2O_4$. The corresponding experimental values have been taken from Refs. 27 and 28.

	x (Expt.)	x (Calc.)	y (Expt.)	y (Calc.)	z (Expt.)	z (Calc.)
α-Al_2O_3 Al					0.3522	0.3521
O	0.3063	0.3076				
$BeAl_2O_4$Al C_s	0.2732	0.2734			0.9941	0.9937
Be	0.0929	0.0926			0.4335	0.4354
O1	0.0905	0.0901			0.7902	0.7954
O2	0.4334	0.4306			0.2410	0.2440
O3	0.1632	0.1628	0.0172	0.0112	0.2585	0.2554

B. Multiplet energy and absorption spectra

The calculations for the multiplet energy levels and absorption spectra were performed with first-principles

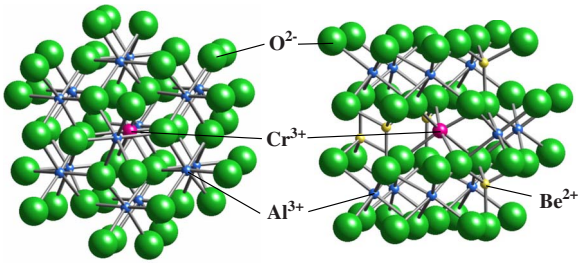

FIG. 2. (Color online) The $CrAl_{14}O_{48}^{51-}$ model cluster for ruby and the $Be_5CrAl_{10}O_{44}^{45-}$ model cluster for alexandrite.

embedded-cluster calculation based on a hybrid method based on DFT and the configuration-interaction (CI) method.[19] The $CrAl_{14}O_{48}^{51-}$ model cluster, which consists of 63 atoms for ruby, and the $Be_5CrAl_{10}O_{44}^{45-}$ model cluster, which consists of 60 atoms for alexandrite, were used for this calculation. The local structures estimated by first-principles method are used for these model clusters. These model clusters are shown in Fig. 2. In addition, an effective Madelung potential was also considered by locating several thousand point charges at atomic sites outside the cluster. We adopted the formal charges 3+ for Al and Cr, 2+ for Be, and 2− for O in the Madelung potential. In previous calculations, clusters of this size and Madelung potential proved to well describe the impurity-state orbitals.[19]

The details of the computational methods employed in this study were originally described in Ref. 19, so we will explain them only briefly here. First-principles molecular-orbital (MO) calculations based on DFT were carried out. The atomic orbitals (AO) were used as basis functions in the MO calculations. Exchange-correlation interactions were considered by using the Dirac-Fock-Slater approximation. We did not use spin polarization in these MO calculations except for the estimation of spin-flip energy, since the spin state was automatically taken into account in the CI calculations. After the one-electron MO calculation, CI calculations were performed to obtain the many-electron wave function and multiplet energy. In these calculations, only electrons occupying the impurity state were considered explicitly. The effective Hamiltonian is generally expressed as

$$H = \sum_{i=1}^{n} h(\mathbf{r}_i) + \sum_{i} \sum_{j<i} g(\mathbf{r}_i, \mathbf{r}_j), \tag{1}$$

where n is the number of electrons in the active space of the CI calculation (in the case of Cr^{3+}, $n=3$) and $\mathbf{r}_i$ is the position of the ith electron. The first and second terms of H represent the one-electron operators and two-electron operators, respectively. The one-electron operator h can be expressed as

$$h(\mathbf{r}) = -\frac{1}{2}\nabla^2 - \sum_{v} \frac{Z_v}{|\mathbf{r}_i - \mathbf{R}_v|} + V_0(\mathbf{r}) + \sum_{\mu} \frac{Z_\mu^{\text{eff}}}{|\mathbf{r}_i - \mathbf{R}_\mu|}, \tag{2}$$

where Z_v and $\mathbf{R}_v$ are the charge and position of the vth nucleus and Z_μ^{eff} and $\mathbf{R}_\mu$ are the effective charge and position of the μth ion outside the model cluster. $V_0(\mathbf{r}_i)$ in Eq. (2) denotes the Coulomb and exchange-correlation potential on these explicitly treated electrons from the other (core and valence) electrons, as proposed by Watanabe and Kamimura.[31] On the other hand, the two-electron operators represent the electron-electron repulsion between the electrons occupying the impurity states

$$g(\mathbf{r}_i, \mathbf{r}_j) = \frac{1}{|\mathbf{r}_i - \mathbf{r}_j|}. \tag{3}$$

This effective many-electron Hamiltonian H is diagonalized within the subspace spanned by the Slater determinants Φ_i constructed from the impurity-state orbitals obtained from the single-electron MO calculation. The matrix element of the effective many-electron Hamiltonian H between two Slater determinants, Φ_p and Φ_q, can be generally expressed as

$$H_{pq} = \langle \Phi_p | H | \Phi_q \rangle = \sum_{i=1}^{L} \sum_{j=1}^{L} A_{ij}^{pq} \langle i|h|j\rangle + \sum_{i=1}^{L} \sum_{j=1}^{L} \sum_{k=1}^{L} \sum_{l=1}^{L} B_{ijkl}^{pq} \langle ij|g|kl\rangle, \tag{4}$$

where L is the number of impurity-state orbitals and A_{ij}^{pq} and B_{ijkl}^{pq} are coefficients. In previous work, we found that the direct diagonalization of the matrix elements of Eq. (4), referred to as the direct matrix calculation (DMC) approach, slightly overestimated the absolute multiplet energy. On the other hand, an introduction of a correction to the barycenter of each configuration, which was referred to as the configuration dependant correction (CDC) approach, was found to be useful for the quantitative estimation of absolute multiplet energy levels. The CDCs were calculated nonempirically from the crystal-field splitting obtained from the one-electron calculation. In order to estimate absolute multiplet energy quantitatively, we adopted the correlation correction (CC) factor c to reduce the overestimation of electron-electron repulsion integrals due to the underestimation of electron correlation effects resulting from the limited number of considered configurations. This factor was also calculated nonempirically from the consistency between the spin-polarized one-electron calculation and the multiplet calculation. In the CDC approach using the CC factor c, the matrix elements of the effective many-electron Hamiltonian between two Slater determinants Φ_p and Φ_q can be expressed as functions of c,

$$H_{pq}^{\text{CDC}}(c) = \langle \Phi_p | H_{pq}^{\text{CDC}} | \Phi_q \rangle = \sum_{i=1}^{L} \sum_{j=1}^{L} A_{ij}^{pq} \langle i|h|j\rangle + \sum_{i=1}^{L} \sum_{j=1}^{L} \sum_{k=1}^{L} \sum_{l=1}^{L} c \times B_{ijkl}^{pq} \langle ij|g|kl\rangle + D_{\text{CDC}}(m,n)\,\delta_{pq}, \tag{5}$$

where m and n are the numbers of electrons occupying the t_{2g} and e_g orbitals in the pth Slater determinant and $D_{\text{CDC}}(m,n)$ is the correction to the diagonal matrix elements of Σh for states belonging to the $t_{2g}^m e_g^n$ configuration. In particular, the $D_{\text{CDC}}(m,n)$ can be expressed as

$$D_{\mathrm{CDC}}(m,n) = n\Delta_{\mathrm{eff}} - \frac{1}{N(m,n)} \sum_{p\in(m,n)} \left\{ \sum_{i=1}^{L}\sum_{j=1}^{L} A_{ij}^{pp}\langle i|h|j\rangle + \sum_{i=1}^{L}\sum_{j=1}^{L}\sum_{k=1}^{L}\sum_{l=1}^{L} B_{ijkl}^{pp}\langle ij|g|kl\rangle \right\}, \quad (6)$$

where Δ_{eff} is the effective crystal-field split defined as the difference between the energies of t_{2g} and e_g states and $N(m,n)$ is the number of Slater determinants belonging to the (m,n) configuration. In order to determine the value of $D_{\mathrm{CDC}}(m,n)$ for each configuration, the contribution of the average value of the electron-electron interaction term should be subtracted. $D_{\mathrm{CDC}}(m,n)$ was determined on the basis of the method of Fazzio, Caldas, and Zunger (FCZ).[32,33] However, one big difference between our approach and the FCZ approach is that the structural distortion from O_h symmetry was considered an off-diagonal matrix element of Σh in our method. In the case of the Cr^{3+} (d^3) ion, the possible configurations (m,n) are (3, 0), (2,1), (1,2), and (0,3), which have 20, 60, 36, and four Slater determinants, respectively. Consequently, the total number of Slater determinants is 120 and the sum of p was taken over all Slater determinants in each configuration. Note that the many-electron CI calculations were performed using accurate MOs corresponding to each crystal field (C_3 for ruby and C_s for alexandrite). Only determinations of $D_{\mathrm{CDC}}(m,n)$ were approximately performed using O_h symmetry notations. A detailed description of these procedures is presented in Ref. 19.

In the DFT-CI calculation, the many-electron wave functions were explicitly obtained as a linear combination of the Slater determinants. Therefore, a direct calculation of transition probability between multiplets was possible. In order to estimate the oscillator strength of the electric-dipole transition for Cr^{3+} in α-Al_2O_3 and $BeAl_2O_4$ host crystal, the general equation of oscillator strength for the electric-dipole transition between the initial and final states was used, which is given by[7]

$$I_{if} = 2(E_f - E_i)\left|\langle \Psi_f | \sum_{k=1}^{n} \mathbf{r}_k \cdot \mathbf{e} | \Psi_i \rangle\right|^2, \quad (7)$$

where Ψ_i and Ψ_f are the respective many-electron wave functions for the initial state and the final state and E_i, E_f are their respective energies. For easy comparison to experimental spectra, each level was broadened to a 0.30 eV full width at half maximum (FWHM) Gaussian function by the following equation:

$$f_i(\varepsilon) = \sum_f \frac{1}{\sqrt{2\sigma^2\pi}} I_{if} \exp\left[-\frac{1}{2\sigma^2}(E - \Delta\varepsilon_{if})^2\right], \quad (8)$$

where I_{if} is oscillator strength, σ is FWHM, E is energy, $\Delta\varepsilon_{if}$ is energy difference between the initial state and the final state, and $(2\sigma^2\pi)^{-1/2}$ is the normalization constant. The initial states i of GSA and ESA were $^4A_1$ and ^2E, respectively. In addition, we also estimated the cross sections of the theoretical absorption spectra and compared them to the experimental ones.

TABLE III. Theoretical and experimental distances between atoms in ruby. (a) The experimental distances between the central Al and surrounding atoms in pure α-Al_2O_3 (Ref. 27). (b) The theoretical distances between the central Al and surrounding atoms in pure α-Al_2O_3. (c) The experimental distances between the central Cr and surrounding atoms in ruby (Ref. 14). (d) The theoretical distances between the central Cr and surrounding atoms in ruby by seven-atom relaxation model. (e) The theoretical distances between the central Cr and surrounding atoms in ruby by 11-atom relaxation model. (d) The theoretical distances between the central Cr and surrounding atoms in ruby by 20-atom relaxation model.

	(a)[a]	(b)		(c)[b]	(d)	(e)	(f)
Al-O1 (Å)	1.854	1.830	Cr-O1 (Å)	1.92	1.901	1.921	1.922
Al-O2 (Å)	1.971	1.954	Cr-O2 (Å)	2.01	1.968	1.982	1.986
Al-Al1 (Å)	2.655	2.628	Cr-Al1 (Å)	2.65		2.618	2.613
Al-Al2 (Å)	2.790	2.754	Cr-Al2 (Å)	2.85		2.765	2.760
Al-Al3 (Å)	3.217	3.183	Cr-Al3 (Å)				3.214
Al-Al4 (Å)	3.497	3.497	Cr-Al4 (Å)				3.485

[a]Reference 27.
[b]Reference 14.

III. RESULTS AND DISCUSSION

A. Lattice relaxation

We first discuss the results of optimized structures for α-Al_2O_3 and $BeAl_2O_4$ host crystal. A global minimum of the energy surface was sought using first-principles total energy and molecular-dynamics methods with the CASTEP code.[25,26] In order to confirm the accuracy of the approach, the lattice parameters and all atomic positions of the unit cell for pure α-Al_2O_3 and $BeAl_2O_4$ were optimized, then compared to their experimental values.[27,28] The theoretical and experimental lattice constants of both crystals are listed in Table I. Since the difference between experimental and theoretical values is about 1%, the optimized structures of the host crystals are considered to be in good agreement with experiment. In addition, the theoretical and experimental internal coordinate parameters are listed in Table II. All parameters reproduce their experimental values reasonably well.

Next, we estimated the optimized structure surrounding doped-Cr^{3+} ions in ruby and alexandrite using the above-mentioned first-principles calculations. In order to estimate the range of the lattice relaxation effect, we estimated the optimized structure in three patterns for ruby and two patterns for alexandrite. The estimated and experimental bond lengths are listed in Table III for ruby and Table IV for alexandrite. The experimental bond lengths of pure host crystals (α-Al_2O_3 and $BeAl_2O_4$) are also listed in Tables III and IV. The local symmetry of the Al site in pure α-Al_2O_3 crystal has C_3 symmetry. The C_3 symmetry of the Cr site was conserved during the geometry optimization of Cr^{3+}-doped α-Al_2O_3 under all conditions. Similarly, the C_s symmetry of the Cr site in alexandrite was also conserved in all geometry optimization calculations. In the case of ruby, our results are consistent with EXAFS analysis and previous DFT calculations, in which the C_3 symmetry of doped-Cr^{3+} site in α-Al_2O_3 was conserved.[14,15,23] Our theoretical estimation of

TABLE IV. Theoretical and experimental distances between atoms of alexandrite. (a) The experimental distances between the central Al and surrounding atoms in pure $BeAl_2O_4$ (Ref. 28). (b) The theoretical distances between the central Al and surrounding atoms in pure $BeAl_2O_4$. (c) The theoretical distances between the central Cr and surrounding atoms in ruby by seven-atom relaxation model. (d) The theoretical distances between the central Cr and surrounding atoms in ruby by 21-atom relaxation model.

	(a)[a]	(b)		(c)	(d)
Al-O1 (Å)	1.862	1.839	Cr-O1 (Å)	1.915	1.922
Al-O2 (Å)	1.894	1.868	Cr-O2 (Å)	1.946	1.953
Al-O3 (Å)	1.941	1.924	Cr-O3 (Å)	1.971	1.978
Al-O4 (Å)	2.017	2.019	Cr-O4 (Å)	2.034	2.037
Al-Al1 (Å)	3.382	3.368	Cr-Al1 (Å)		3.390
Al-Al2 (Å)	3.548	3.533	Cr-Al2 (Å)		3.547
Al-Al3 (Å)	3.354	3.333	Cr-Al3 (Å)		3.386
Al-Al4 (Å)	2.911	2.892	Cr-Al4 (Å)		2.870
Al-Al5 (Å)	3.548	3.533	Cr-Al5 (Å)		3.531
Al-Be1 (Å)	2.580	2.581	Cr-Be1 (Å)		2.540
Al-Be2 (Å)	3.005	2.990	Cr-Be2 (Å)		3.004
Al-Be3 (Å)	3.025	2.990	Cr-Be3 (Å)		3.049
Al-Be4 (Å)	3.024	3.004	Cr-Be4 (Å)		3.038

[a]Reference 28.

each bond length was in reasonable agreement with experimental values. The slight difference from the theoretical results of Refs. 14 and 15 arose from a difference in calculation conditions. The pseudopotential type was significantly different, as we adopted the ultrasoft pseudopotentials throughout this work instead of the norm-conserving pseudopotentials used in Refs. 14 and 15. In addition, the optimization range also affected the slight difference in calculated bond lengths.

Cr-O bond lengths in alexandrite have not been reported to our knowledge, neither from experiment nor estimated by DFT calculation. However, since the chemical bond properties of Al-O bonds in $BeAl_2O_4$ are similar to those in α-Al_2O_3 even though $BeAl_2O_4$ contains Be-centered tetrahedra,[34] we expected the optimized structure to be in reasonable agreement with the true local structure in alexandrite. For confirmation, we also calculated the relaxation around Cr at the C_i site using a 21-atom optimization model. After optimization, C_i symmetry was preserved and the three types of Cr-O bond lengths changed from 1.861, 1.892, and 1.917 Å to 1.923, 1.948, and 1.959 Å. These displacement magnitudes are similar to those of the C_s site.

For ruby, although the calculated Cr-O bond lengths by seven-atom optimization were underestimated, the calculated Cr-O bond lengths by 11-atom and 20-atom optimizations were almost the same and in reasonable agreement with experimental values.[14]

For alexandrite, on the other hand, the calculated Cr-O bond lengths by seven-atom and 21-atom optimizations were similar. This is probably because of the smaller effect of lattice relaxation of second-nearest-neighbor Al atoms in alexandrite than in ruby due to longer Cr-Al distances.

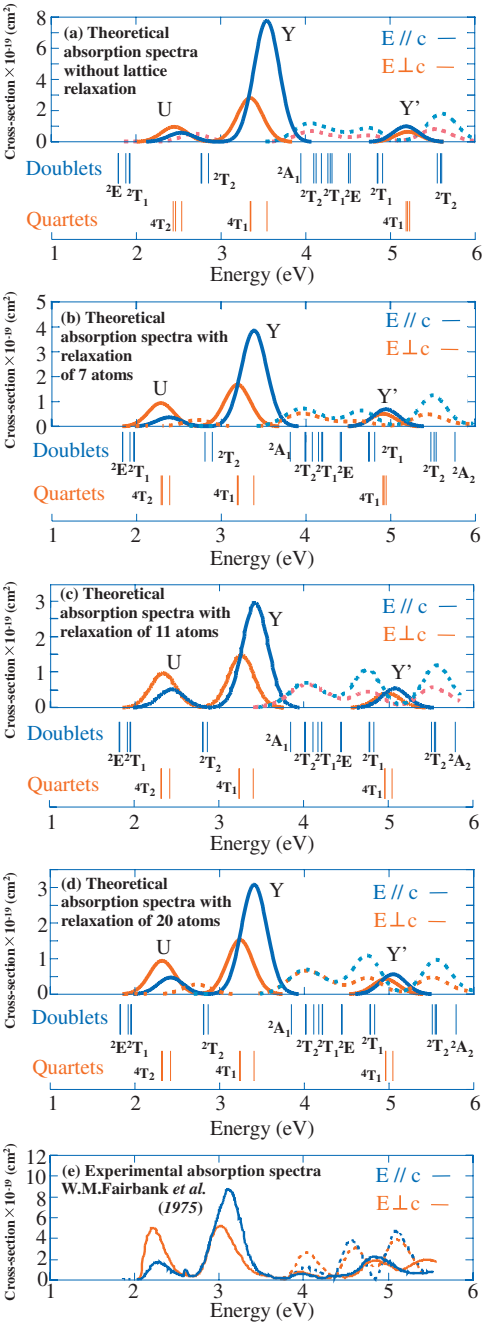

FIG. 3. (Color) Theoretical and experimental GSA (solid line) and ESA from the ^2E (dashed line) spectra of ruby. The red and blue lines represent $E \perp c$ and $E \| c$ spectra, respectively. (a) The theoretical GSA and ESA spectra without lattice relaxation. (b) The theoretical GSA and ESA by seven-atom relaxation model. (c) The theoretical GSA and ESA spectra by 11-atom relaxation model. (d) The theoretical GSA and ESA spectra by 20-atom relaxation model. (e) The experimental GSA and ESA spectra (Ref. 35).

B. Multiplet energy levels and absorption spectra of ruby

In order to confirm the accuracy of estimated structures and investigate the range of lattice relaxation effects, we calculated the GSA and ESA spectra from the ^2E state as well as the multiplet energy levels by first-principles CI method using the optimized ruby structures. Figure 3 shows calculated

TABLE V. The multiplet energy levels of ruby corresponding to the GSA together with the peak positions of the observed absorption spectra of ruby reported by Uimin and Brenig (Ref. 35). The final states of GSA are also listed.

	^2E(R) (eV)	$^2T_1$(R′) (eV)	$^2T_2$(B) (eV)	$^4T_2$(U) (eV)	$^4T_{1a}$(Y) (eV)	$^4T_{1b}$(Y′) (eV)
Unrelax	1.79	1.88	2.76	2.44(σ)	3.34(σ)	5.20(σ)
	1.79	1.92	2.77	46(σ)	3.35(σ)	5.23(σ)
		1.93	2.85	2.54(π)	3.54(π)	5.18(π)
7-atom relax	1.82	1.92	2.81	2.28(σ)	3.18(σ)	4.91(σ)
	1.83	1.96	2.81	2.29(σ)	3.20(σ)	4.91(σ)
		1.97	2.88	2.38(π)	3.39(π)	4.95(π)
11-atom relax	1.83	1.92	2.81	2.33(σ)	3.26(σ)	4.99(σ)
	1.83	1.95	2.82	2.34(σ)	3.26(σ)	4.99(σ)
		1.96	2.87	2.44(π)	3.42(π)	5.07(π)
20-atom relax	1.82	1.92	2.81	2.32(σ)	3.24(σ)	4.96(σ)
	1.83	1.95	2.81	2.32(σ)	3.24(σ)	4.96(σ)
		1.96	2.87	2.42(π)	3.41(π)	5.05(π)
Experiment[a]	1.79	1.85	2.60	2.23(σ)	3.01(σ)	4.84(σ)
	1.79	1.88	2.61	2.28(π)	3.11(π)	4.84(π)
		1.88	2.65			

[a]Reference 35.

GSA and ESA spectra and multiplet energy levels for ruby. The multiplet energy levels corresponding to the GSA and ESA from ^2E are also listed in Tables V and VI, respectively. The experimental GSA and ESA spectra are also shown in panel (e).[35] The solid and dashed lines represent the GSA and ESA spectra, respectively. We note that the ESA spectra are shifted so that their origins are located at the position of the ^2E state, enabling easy comparison between the energy levels and the spectra. The GSA spectra have three broad bands and three sharp lines, which were attributed to transitions from $^4A_2$ to $^4T_2$ (U band), $^4T_1$ (Y band), $^4T^1$ (Y′ band), ^2E (R line), $^2T_1$ (R′ line), and $^2T_2$ (B line). The ESA spectra from ^2E have three broad bands, which were attributed to transitions from ^2E to $^2T_2$ and $^2T_1$, $^2T_1$, and $^2T_2$ from the lower level. These attributions are also listed in Tables V and VI.

Next, we discuss the calculated absorption spectra without lattice relaxation, as shown in panel (a). There are three major differences between the experimental and the theoretical absorption spectra without lattice relaxation. First, the intensity ratio of the U band to the Y band was different. The intensity of the U band relative to that of the Y band was too weak in the theoretical spectrum. Second, the peak energy was different. The absolute multiplet energies were slightly overestimated. Finally, the intensity ratio of ESA spectra had three clearly observable peaks in the experimental spectrum, but these were not clearly visible in the theoretical spectrum. These three major differences were assumed to be due to the lattice relaxation effect around the doped Cr^{3+}. Compared to Ref. 19, the absolute value of intensity for the U band was different. Because the numerical integrals were improved significantly by increasing the number of sample points, the intensity of the Y band in the present work was improved relative to that calculated in Ref. 19.

Therefore, we also calculated the GSA and ESA spectra and multiplet structure of ruby using the optimized structures. These spectra and multiplet energy levels are also shown in Fig. 3. Panels (b), (c), and (d) show the theoretical absorption spectra and multiplet energy levels calculated using the structures obtained from the seven-, 11-, and 20-atom relaxation models, respectively.

TABLE VI. The multiplet energy levels of ruby corresponding to the ESA together with the peak positions in the observed absorption spectra of ruby reported by Uimin and Brenig (Ref. 35). The final states of ESA are also listed.

	$^2T_2$, $^2T_1$ (eV)	$^2T_1$ (eV)	$^2T_2$ (eV)
	Unrelax		
(σ)	4.21	4.91	5.55
(π)	4.21	4.85	5.59
	7-atom relax		
(σ)	4.09	4.80	5.47
(π)	4.09	4.74	5.52
	11-atom relax		
(σ)	4.14	4.85	5.51
(π)	4.14	4.80	5.56
	20-atom relax		
(σ)	4.12	4.83	5.53
(π)	4.12	4.78	5.57
	Experiment[a]		
(σ)	4.04	4.60	5.08
(π)	4.03	4.55	5.08

[a]Reference 35.

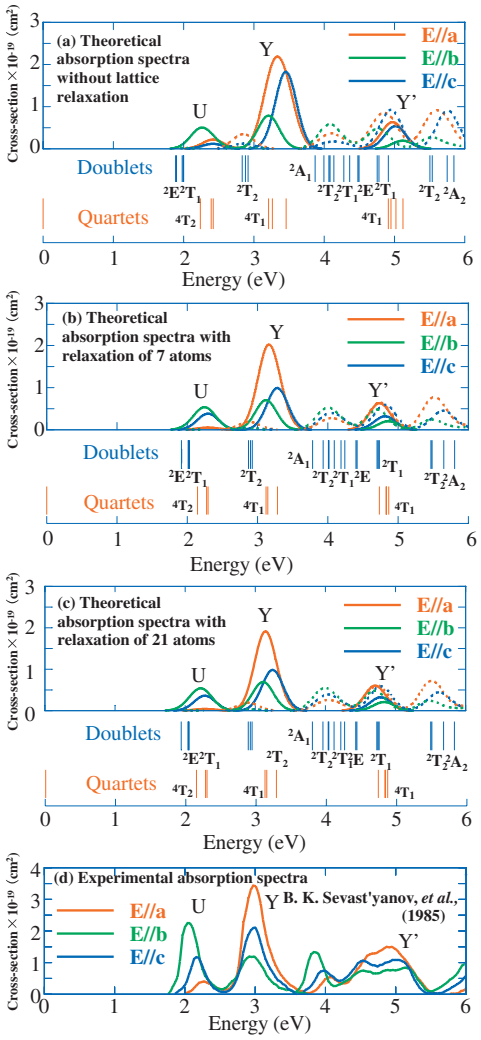

FIG. 4. (Color) Theoretical and experimental GSA and ESA from the ^2E spectra of alexandrite. The red, green, and blue lines represent $E\|a$, $E\|b$, and $E\|c$ spectra, respectively. For theoretical spectra, the solid and dashed lines represent the GSA and ESA, respectively. (a) The theoretical GSA and ESA spectra without lattice relaxation. (b) The theoretical GSA and ESA spectra by seven-atom relaxation model. (c) The theoretical GSA and ESA spectra by 21-atom relaxation model. (d) The experimental GSA and ESA spectra (Ref. 37).

In the theoretical spectra from the seven-atom relaxation model, in which the lattice relaxation of the central Cr and nearest six O atoms were considered, although the theoretical spectra were basically the same, the U band to Y band intensity ratio was slightly improved. On the other hand, in the theoretical spectra from the 11-atom and 20-atom relaxation models, the absolute peak energies, the intensity ratio of U band to Y band, and the overall structure of ESA were all improved and are in good agreement with the experimental results. In addition, the order of the cross section of absorption intensity was also reasonably well reproduced by the first-principles CI calculation.

We could not find a clear difference between the 11-atom and 20-atom relaxation models. Thus, we concluded that the absolute multiplet energy and overall structure of absorption spectra were in good agreement with the experimental values when using the 11-atom lattice relaxation, which considered the lattice relaxation of the doped Cr atom, the nearest six O atoms, and the nearest four Al atoms. As mentioned above, this conclusion is consistent with the results of lattice relaxation estimation by first-principles calculation.

Finally, the experimental spectrum exhibited peaks at ca. 4 and 5.5 eV, which were not present in the theoretical spectra. We presume that the peak at 4 eV originated from some sort of contamination because there was no peak at 4 eV in the previous experimental spectra reported by McClure.[36] On the other hand, the peak at 5.5 eV was attributed to the charge-transfer state in that experiment.[36] Since we did not consider the CT state in the present calculation, the peak at 5.5 eV is not present in our theoretical calculations.

C. Multiplet energy levels and absorption spectra of alexandrite

We also calculated the GSA and ESA spectra and multiplet energy levels by a first-principles CI method using the optimized structures for alexandrite. Since the space group of the chrysoberyl is *Pnma*, three independent absorption spectra were observed. Figure 4 shows the calculated GSA and ESA spectra and multiplet energy levels for alexandrite. The multiplet energy levels corresponding to the GSA and ESA from ^2E are also listed in Tables VII and VIII, respectively. The experimental GSA and ESA spectra are also shown in panel (d).[37] The experimental spectra of alexandrite cannot be divided into GSA and ESA, so both spectra were drawn as solid lines. On the other hand, in the theoretical spectra, the solid line and dashed lines represent the GSA and ESA spectra, respectively. As in the ruby results, the ESA spectra were shifted to set their origin at the position of the ^2E state for easy comparison between the energy levels and the spectra. The origin of each transition is similar to those of ruby, and these attributions are also listed in Tables VII and VIII.

Panel (a) shows the calculated GSA and ESA spectra without lattice relaxation. For alexandrite, theoretical absorption spectra reasonably reproduced experimental ones, even when the lattice relaxation was not considered. However, there were a few minor differences between the experimental and theoretical spectra. The polarization dependence of the U band was not well reproduced. The intensity of the $E\|a$ spectrum was stronger than that of the $E\|c$ spectrum in the theoretical calculations, however, the opposite relationship was observed in the experimental U band. The peak energy of the Y band in the $E\|c$ spectrum was slightly overestimated in the theoretical spectra. Also, the polarization dependence of the ESA did not reproduce the experimental ESA spectra, where the relative intensities of $E\|a$ and $E\|c$ of the first ESA peak were opposite. As with ruby, these differences originate from underestimation of the Cr-O bond length.

Therefore, we also calculated the GSA and ESA spectra and multiplet structure of alexandrite using the optimized structures. The calculated spectra and multiplet energy levels are shown in Fig. 4. Panels (b) and (c) show the theoretical absorption spectra and multiplet energy levels resulting from consideration of the relaxation of seven atoms and 21 atoms by first-principles calculation, respectively. Theoretical spec-

TABLE VII. The multiplet energy levels of alexandrite corresponding to the GSA together with the peak positions in the observed absorption spectra of ruby reported by Sevast'yanov *et al.* (Ref. 37). The final states of GSA are also listed.

	^2E(R) (eV)	$^2T_1$(R′) (eV)	$^2T_2$(B) (eV)	$^4T_2$(U) (eV)	$^4T_{1a}$(Y) (eV)	$^4T_{1b}$(Y′) (eV)
Unrelax	1.89	1.98	2.84	2.42($E\|\|a$)	3.27($E\|\|a$)	4.95($E\|\|a$)
	1.89	1.99	2.88	2.24($E\|\|b$)	3.21($E\|\|b$)	5.12($E\|\|b$)
		2.00	2.92	2.39($E\|\|c$)	3.46($E\|\|c$)	5.02($E\|\|c$)
7-atom relax	1.92	2.01	2.87	2.30($E\|\|a$)	3.16($E\|\|a$)	4.76($E\|\|a$)
	1.92	2.02	2.90	2.14($E\|\|b$)	3.12($E\|\|b$)	4.88($E\|\|b$)
		2.03	2.93	2.28($E\|\|c$)	3.29($E\|\|c$)	4.83($E\|\|c$)
21-atom relax	1.93	2.02	2.88	2.28($E\|\|a$)	3.13($E\|\|a$)	4.71($E\|\|a$)
	1.93	2.03	2.92	2.13($E\|\|b$)	3.11($E\|\|b$)	4.84($E\|\|b$)
		2.04	2.93	2.26($E\|\|c$)	3.25($E\|\|c$)	4.80($E\|\|c$)
Experiment[a]	1.82	1.89	2.63	2.19($E\|\|a$)	2.96($E\|\|a$)	4.71($E\|\|a$)
	1.83	1.91	2.65	2.10($E\|\|b$)	2.96($E\|\|b$)	4.71($E\|\|b$)
		1.92	2.69	2.17($E\|\|c$)	2.99($E\|\|c$)	5.01($E\|\|b$)
						4.65($E\|\|c$)

[a]Reference 37.

tra calculated by seven-atom and 21-atom relaxation models well reproduced the experimental results. The polarization dependences of U and Y bands and ESA spectra were improved considerably and reproduced the experimental tendencies fairly well without the use of any empirical parameters. In addition, the order of the cross section of absorption intensity was reasonably well reproduced by the first-principles CI calculation.

TABLE VIII. The multiplet energy levels of alexandrite corresponding to the ESA together with the peak positions in the observed absorption spectra of ruby reported by Sevast'yanov *et al.* (Ref. 37). The final states of ESA are also listed.

	$^2T_2$, $^2T_1$ (eV)	$^2T_1$ (eV)	$^2T_2$ (eV)
	Unrelax		
$E\|\|a$	4.04	4.64	4.92
$E\|\|b$	3.89	4.59	4.92
$E\|\|c$	4.02	4.59	5.22
	7-atom relax		
$E\|\|a$	4.08	4.78	5.54
$E\|\|b$	4.07	4.75	5.50
$E\|\|c$	4.13	4.91	5.75
	21-atom relax		
$E\|\|a$	4.09	4.72	5.48
$E\|\|b$	4.01	4.70	5.47
$E\|\|c$	4.02	4.74	5.65
	Experiment[a]		
$E\|\|a$	4.08	4.70	5.49
$E\|\|b$	4.01	4.70	5.47
$E\|\|c$	4.02	4.70	5.63

[a]Reference 37.

We could not find a clear difference between the seven-atom and 21-atom relaxation models. Thus, we concluded that the absolute multiplet energy and overall structure of absorption spectra were in good agreement with experimental results when seven-atom lattice relaxation was considered, which included the lattice relaxation of a central Cr and the six nearest-neighbor O atoms. This conclusion is consistent with the results of lattice relaxation estimation for ruby, since the distance between the central Cr and the nearest Al atoms is greater than 2.8 Å, much greater than of the distances in ruby. These results indicate that the overall features of the experimental spectra for both ruby and alexandrite were well reproduced by considering lattice relaxations within a range of about 2.8 Å.

IV. CONCLUSION

We investigated the GSA and ESA spectra of ruby and alexandrite using a first-principles method that included lattice relaxations. The optimized local structure around the doped-Cr^{3+} ion in ruby and alexandrite was determined by first-principles DFT calculations based on the band-structure approach. The results of geometry optimization calculations indicated that the local symmetry of the Cr site in both ruby and alexandrite preserved the original C_3 and C_s point symmetry. In ruby, the optimized bond lengths were in good agreement with experimental values.

The GSA and ESA spectra and multiplet energy levels for both ruby and alexandrite were calculated by a first-principles CI method using both unrelaxed and optimized structures. In the case of ruby, the ratios of the peak intensity and the peak position were improved by considering the relaxation of 11 or more atoms. ESA spectra were dramatically improved. For alexandrite, the polarization dependence of the U band was significantly improved by considering the relaxation of seven or more atoms. Thus, we conclude that

the overall features of the experimental spectra for both ruby and alexandrite were well reproduced by including lattice relaxations within a range of about 2.8 Å from the central Cr atom.

We calculated the GSA and ESA spectra of ruby and alexandrite by a first-principles method with reasonable agreement with experimental observations. However, since a relativistic version of the CDC program is not available at the present time, we could not estimate spin-forbidden transitions such as the transition from quartet to doublet, nor could we calculate the spin-orbit interactions. We believe that inclusion of these effects would improve the agreement between calculated and experimental optical properties. Finally, we believe that the effectiveness of first-principles CI calculation combined with structural optimization using a first-principles total-energy calculation as a tool to analyze optical materials such as solid-state lasers or phosphors was clearly demonstrated by successful calculation of GSA and ESA for ruby and alexandrite.

ACKNOWLEDGMENTS

The authors are grateful to H. Moriwake for useful discussion of band-structure calculation. The present work was partially supported by the "Open Research Center" Project for Private Universities matching fund subsidy from MEXT (Ministry of Education, Culture, Sports, Science, and Technology).

[1] T. H. Maiman, Nature (London) **187**, 493 (1960).
[2] R. A. Forman, G. J. Piermarini, J. D. Barnett, and S. Block, Science **176**, 284 (1972).
[3] J. H. Eggert, K. A. Goettel, and I. F. Silvera, Phys. Rev. B **40**, 5724 (1989).
[4] J. H. Eggert, F. Moshary, W. J. Evans, K. A. Goettel, and I. F. Silvera, Phys. Rev. B **44**, 7202 (1991).
[5] J. Lin, O. Degtyareva, C. T. Prewitt, P. Dera, N. Sata, E. Gregoryanz, H. Mao, and R. J. Hemley, Nature Mater. **3**, 389 (2004).
[6] J. C. Walling, O. G. Peterson, H. P. Jenssen, R. C. Morris, and E. Wayne O'Dell, IEEE J. Quantum Electron. **16**, 1302 (1980).
[7] S. Sugano, Y. Tanabe, and H. Kamimura, *Multiplets of Transition-Metal Ions in Crystals* (Academic, New York, 1970).
[8] W. Duan, R. M. Wentzcovitch, and K. T. Thomson, Phys. Rev. B **57**, 10363 (1998).
[9] V. V. Mazurenko, A. N. Varaksin, V. G. Mazurenko, V. S. Kortov, and V. I. Anisimov, Physica B **344**, 385 (2004).
[10] J. M. García-Lastra, M. T. Barriuso, J. A. Aramburu, and M. Moreno, Phys. Rev. B **72**, 113104 (2005).
[11] J. M. García-Lastra, J. A. Aramburu, M. T. Barriuso, and M. Moreno, Phys. Rev. B **74**, 115118 (2006).
[12] M. Moreno, M. T. Barriuso, J. A. Aramburu, P. García-Fernández, and J. M. Garcia-Lastra, J. Phys.: Condens. Matter **18**, R315 (2006).
[13] E. Gaudry, D. Cabaret, C. Brouder, I. Letard, A. Rogalev, F. Wilhlem, N. Jaouen, and P. Sainctavit, Phys. Rev. B **76**, 094110 (2007).
[14] E. Gaudry, A. Kiratisin, P. Sainctavit, C. Brouder, F. Mauri, A. Ramos, A. Rogalev, and J. Goulon, Phys. Rev. B **67**, 094108 (2003).
[15] E. Gaudry, D. Gabarer, P. Sainctavit, C. Brouder, F. Mauri, J. Goulon, and A. Rogalev, J. Phys.: Condens. Matter **17**, 5467 (2005).
[16] A. C. Lewandowski and T. M. Wilson, Phys. Rev. B **50**, 2780 (1994).
[17] W. Duan, G. Paiva, R. M. Wentzcovitch, and A. Fazzio, Phys. Rev. Lett. **81**, 3267 (1998).
[18] L. Seijo and Z. Barandiarán, in *Computational Chemistry: Reviews of Modern Trends*, edited by J. Leszczynski (World Scientific, Singapore, 1999), Vol. 4, Chap. 2.
[19] K. Ogasawara, T. Ishii, I. Tanaka, and H. Adachi, Phys. Rev. B **61**, 143 (2000).
[20] T. Ishii, K. Ogasawara, H. Adachi, and I. Tanaka, J. Phys. Chem. **115**, 492 (2001).
[21] J. L. Pascual, B. Savoini, and R. Gonzalez, Phys. Rev. B **70**, 045109 (2004).
[22] R. D. Shannon, Acta Crystallogr., Sect. A: Cryst. Phys., Diffr., Theor. Gen. Crystallogr. **32**, 751 (1976).
[23] E. Gaudry, P. Sainctavit, F. Juillot, F. Bondioli, P. Ohresser, and I. Letard, Phys. Chem. Miner. **32**, 710 (2006).
[24] W. Y. Ching and Y. N. Xu, J. Am. Ceram. Soc. **77**, 404 (1994).
[25] M. C. Payne, M. P. Teter, D. C. Allan, T. A. Arias, and J. D. Joannopoulos, Rev. Mod. Phys. **64**, 1045 (1992).
[26] M. D. Segall, P. J. D. Lindan, M. J. Probert, C. J. Pickard, P. J. Hasnip, S. J. Clark, and M. C. Payne, J. Phys.: Condens. Matter **14**, 2717 (2002).
[27] S. Pillet, M. Souhassou, C. Lecomte, K. Schwarz, P. Blaha, M. Rérat, A. Lichanot, and P. Rpversi, Acta Crystallogr., Sect. A: Found. Crystallogr. **57**, 290 (2001).
[28] E. F. Farrell, J. H. Fang, and R. E. Newnham, Am. Mineral. **48**, 804 (1963).
[29] D. Vanderbilt, Phys. Rev. B **41**, 7892 (1990).
[30] J. P. Perdew, K. Burke, and M. Ernzerhof, Phys. Rev. Lett. **77**, 3865 (1996).
[31] S. Watanabe and K. Kamimura, Mater. Sci. Eng., B **3**, 313 (1989).
[32] A. Fazzio, M. Caldas, and A. Zunger, Phys. Rev. B **29**, 5999 (1984).
[33] A. Fazzio, M. J. Caldas, and A. Zunger, Phys. Rev. B **30**, 3430 (1984).
[34] W. Y. Ching, Y. N. Xu, and B. K. Brickeen, Phys. Rev. B **63**, 115101 (2001).
[35] W. M. Fairbank, Jr., G. K. Klauminzer, and A. L. Schawlow, Phys. Rev. B **11**, 60 (1975).
[36] D. S. McClure, J. Chem. Phys. **36**, 2757 (1962).
[37] B. K. Sevast'yanov, Y. L. Remigailo, T. F. Veremeichik, and B. P. Orekhova, Sov. Phys. Dokl. **30**, 1051 (1985).